International Journal of Developmental Neuroscience 76 (2019) 34–40

Contents lists available at ScienceDirect

International Journal of Developmental Neuroscience

journal homepage: www.elsevier.com/locate/ijdevneu

The left lateral occipital cortex exhibits decreased thickness in children with sensorineural hearing loss

Tadashi Shiohama[a,b,*], Jeremy McDavid[a], Jacob Levman[a,c], Emi Takahashi[a]

[a] Division of Newborn Medicine, Department of Medicine, Boston Children's Hospital, Harvard Medical School, 300 Longwood Avenue, Boston, MA, 02115, USA
[b] Department of Pediatrics, Chiba University Hospital, Inohana 1-8-1, Chiba-shi, Chiba, 2608670, Japan
[c] Department of Mathematics, Statistics and Computer Science, St. Francis Xavier University, 2323 Notre Dame Ave, Antigonish, Nova Scotia, B2G 2W5, Canada

ARTICLE INFO

Keywords:
Sensorineural hearing loss
Lateral occipital cortex
Brain MRI
Human motion-sensitive middle temporal area
Lateral occipital area
Occipital face area

ABSTRACT

Patients with sensorineural hearing loss (SNHL) tend to show language delay, executive functioning deficits, and visual cognitive impairment, even after intervention with hearing amplification and cochlear implants, which suggest altered brain structures and functions in SNHL patients. In this study, we investigated structural brain MRI in 30 children with SNHL (18 mild to moderate [M-M] SNHL and 12 moderately severe to profound [M–P] SNHL) by comparing gender- and age-matched normal controls (NC). Region-based analyses did not show statistically significant differences in volumes of the cerebrum, basal ganglia, cerebellum, and the ventricles between SNHL and NC. On surface-based analyses, the global and lobar cortical surface area, thickness, and volumes were not statistically significantly different between SNHL and NC participants. Regional surface areas, cortical thicknesses, and cortical volumes were statistically significantly smaller in M–P SNHL compared to NC in the left middle occipital cortex, and left inferior occipital cortex after a correction for multiple comparisons using random field theory ($p < 0.02$). These regions were identified as areas known to be related to high level visual cognition including the human middle temporal area, lateral occipital area, occipital face area, and V8. The observed regional decreased thickness in M–P SNHL may be associated with dysfunctions of visual cognition in SNHL detectable in a clinical setting.

1. Introduction

Hearing loss is the most common developmental sensory disorder with incidence rates of 1.7 and 2.2 per thousand during infancy (Centers for Disease Control and Prevention, 2016) and school ages (Holzinger et al., 2016), respectively. Sensorineural hearing loss (SNHL) is a loss of function within the inner ear or its connections to the brain, and accounts for over 50% of children with hearing loss (Swanepoel de et al., 2013; Martines et al., 2013).

Due to the implementation of ear function screening in newborns, it is now possible to identify hearing loss from birth onwards. Despite advances in screening and cochlear implantation (Monshizadeh et al., 2018), there are still many children with hearing loss that suffer from speech and language problems for a variety of reasons, including delayed diagnosis/intervention, failed follow-up, sporadic attendance of auditory-verbal therapy, and decision not to use hearing aids (Lü et al., 2011; Fitzpatrick et al., 2017). Additionally, even after intervention with hearing amplification and cochlear implants, SNHL places children at risk for language delay (Tomblin et al., 2015; Yoshinaga-Itano et al., 2017), executive functioning deficits (Kronenberger et al., 2014), and visual cognitive impairment (Dye and Hauser, 2014; Turgeon et al., 2012), leading to life-long consequences for affected children.

Language delay and cognitive dysfunction that persist after intervention are likely to be associated with altered brain structure and function in SNHL patients. Therefore, studying detailed changes in the patient brain is critical for understanding their brain development and towards elucidating basic mechanisms of neuroplasticity that can explain abnormal brain function as well as patient clinical courses. However, there have been only a few studies of structural brain magnetic resonance imaging (MRI) in both adults (Shibata, 2007; Hribar et al., 2014; Li et al., 2013) and children (Li et al., 2012) with SNHL. In this study, we investigated structural brain MRI in 30 children with

Abbreviations: SNHL, sensorineural hearing loss; NC, normal controls; M-M, mild to moderate; M–P, moderately severe to profound; YO, years old; GM, gray matter; WM, white matter; GI, gyrification index; mOC, middle occipital cortex; iOC, inferior occipital cortex; RFT, random field theory; hMT, human motion-sensitive middle temporal area; LO, lateral occipital area; OFA, occipital face area

* Corresponding author at: Boston Children's Hospital, 300 Longwood Avenue, Boston, MA, 02115, United States.
E-mail addresses: asuha_hare@yahoo.co.jp, Tadashi.Shiohama@childrens.harvard.edu (T. Shiohama).

https://doi.org/10.1016/j.ijdevneu.2019.05.009
Received 22 January 2019; Received in revised form 10 May 2019; Accepted 30 May 2019
Available online 04 June 2019

SNHL by comparison with normal controls (NC), to help identify abnormal characteristics of the brain morphology in SNHL children.

2. Methods and materials

2.1. Patients

After approval by the Institutional Review Board at Boston Children Hospital (BCH), we reviewed electronic medical records from January 1 st, 2008 to February 24th, 2016, to assemble our listing of SNHL patients. We carefully identified prelingual SNHL participants according to audiometric tests and otolaryngological examinations. The degree of SNHL was determined as mild to moderate (M-M, 26–55 dB HL) and moderately severe to profound (M–P, over 56 dB HL), according to the average of hearing thresholds at 500, 1000, and 2000 Hz for pure tone tests for their better ear or sound-field visual reinforcement audiometry tests for patients that have difficulty being examined by the pure tone tests (Yoshinaga-Itano et al., 2017). We carefully excluded patients with congenital disorders (Down syndrome, CHARGE syndrome, and other chromosomal abnormalities), and perinatal brain damage (hypoxic ischemic encephalopathy, and infarction). The gender- and age-matched NC were selected from our in-house database composed of electronic records of healthy participants without neurological disorders, neuropsychological disorders or epilepsy (Levman et al., 2017). Both datasets (SNHL and NC) were comprised of examinations acquired at BCH on the same suite of MRI scanners.

2.2. Structural MRI acquisition and processing

The MR scanning was performed in SNHL and NC participants under natural sleep or sedation. The quality of the acquired images were visually checked, and images with poor quality were excluded from the analysis despite motion correction. Three-dimensional (3-D) T1-weighted structural brain images (The majority of images in this study was acquired with MP-RAGE. Repetition time [TR] 2000–2500 ms, echo time [TE] 1.7–2.5 ms, inversion time [TI] 800-1,450 ms, voxel size 0.85–1 × 0.85–1 x 1 mm, matrix 256 × 256) were obtained from all participants included in this study with clinical 3 T MRI scanners (Skyra, Siemens Medical Systems, Erlangen, Germany).

Both SNHL and NC participants ware imaged with the same model of clinical 3 T MRI scanners (Skyra, Siemens Medical Systems, Erlangen, Germany) at BCH. Four MRI scanners (“Scanner 1″, “Scanner 2″, “Scanner 3″, and “Scanner 4″) were used for this study. The images were obtained with “Scanner 1″ in 20/30 and 51/90, “Scanner 2″ in 5/30 and 22/90, “Scanner 3″ in 2/30 and 6/90, and “Scanner 4″ in 3/30 and 11/90, in SNHL and NC participants, respectively. There was no statistically significant difference in the rate of MRI scanners in SNHL and NC participants (Pearson Chi-Square test, $\chi 2(4) = 3.872$, $P = 0.424$).

DICOM files were collected through the Children’s Research and Integration System (Pienaar et al., 2015), and analyzed with CIVET version 2.1.0 pipeline (Zijdenbos et al., 2002) on the CBRAIN platform (Sherif et al., 2015). Corrections for non-uniform intensity artifacts by the N3 algorithm (Sled et al., 1998), stereotaxic registration (onto the icbm152 non-linear 2009 template) (Fonov et al., 2009), and brain masking (Smith, 2002) were performed. A region-based volumetric analysis was performed with tissue classification using an artificial neural network classifier (INSECT) (Tohka et al., 2004), and segmentation of brain regions was performed with ANIMAL (Collins et al., 1999).

For the surface-based analysis, the surfaces of the gray matter and white matter were extracted by using 40,962 vertices per hemisphere with the t-laplace metric (Kim et al., 2005; Boucher et al., 2009), and cortical surface parameters including the gyrification index, average cortex thickness, cortical surface area, and cortical volumes were calculated in each hemisphere. The basic lobar surface parcellation and Automated Anatomical Labelling (AAL) surface parcellation (Lyttelton et al., 2007) was used for registration to the anatomical regions. The quality of the outputs of the CIVET pipeline (shapes of the brain mask, linear/non-linear registration to the template, tissue classification, and brain segmentation) were manually inspected for quality.

2.3. Statistical analyses

Each brain structural measurement in SNHL and NC participants were evaluated through Levene’s test for equality of variances and the two-tailed unpaired *t*-test for equality of means. According to the false discovery rate correction for multiple comparisons by the Benjamini-Hochberg procedure (Benjamini et al., 2001), Benjamini-Hochberg critical values ($\alpha = 0.05$, $q = 0.15$) were determined for 57 and 40 repeating *t*-tests in surface- and region-based measurements, respectively. IBM SPSS Statistics version 19 (IBM Corp. Armonk, NY) was used for the statistical analysis. Regional cortical thickness was statistically analyzed and visualized as t-statistic maps and random field theory (RFT) maps (corrected for multiple comparisons) using the SurfStat toolbox (http://www.math.mcgill.ca/keith/surfstat/) on MATLAB R2016a (MathWorks, Natick, MA).

3. Results

3.1. Participants’ background

Our study included 30 SNHL (19 males and 11 females) and 90 NC (57 males and 33 females) participants. The mean ages and [standard deviation (SD)] at MRI examination were 5.3 [4.0] and 5.3 [3.9] years old (YO) in SNHL and NC participants, respectively. The degrees of SNHL were M-M in 18 (60%) and M–P in 12 (40%) among the 30 SNHL participants. The SNHL symptoms were treated with hearing aids only in 23 (77%) and cochlear implants in 5 (17%) patients. Five (17%) patients were born prematurely. As additional comorbidities, epilepsy, Autism spectrum disorder, Attention deficit hyperactivity disorder, and global developmental delay were observed in 2 (7%), 4 (13%), 2 (7%), and 2 (7%) of SNHL participants, respectively.

The 12 M–P SNHL (8 males and 4 females) were compared with selected NC participants (M–P NC) (24 males and 12 females). The mean ages and [SD] at MRI examination were 6.7 [5.2] and 6.7 [5.0] YO in M–P SNHL and M–P NC participants, respectively. There was no statistically significant difference in the examination age (mean [SD] 4.4 [2.6] YO in M-M and 6.7 [5.0] YO in M–P SNHL patients, Student *t* test, $T(28) = -1.56$, $P = 0.13$) and the proportion of male (11/18 in M-M and 8/12 in M–P SNHL patients, Pearson Chi-Square test, $\chi^2(1) = 0.096$, $P = 0.757$).

3.2. Qualitative study

Gross structural abnormalities were not observed in both SNHL and NC participants, however, non-specific spotty lesions with T2-weighted elongation were observed in subcortical white matter (WM) in 2 SNHL participants (Suppl. Fig. 1).

3.3. Region-based volumetric analysis

Global and regional volumes in the cerebrum, basal ganglia, cerebellum, and ventricles did not show statistically significant differences between SNHL and NC participants (Tables 1 and 2), or between M–P SNHL and M–P NC participants (Suppl, Table 1 and 2).

3.4. Surface-based cortical analysis

The surface-based analyses showed that the global gyrification index, surface area, cortical thickness, and cortical volumes were not statistically significantly different between SNHL and NC participants

Table 1
The brain volume of SNHL and NC participants.

Classification	SNHL (N = 30) Mean [SD]	NC (N = 90) Mean [SD]	The rate of SNHL/NC	Absolute Cohen's *d*	*p*
CSF (mm^3)	30,866 [10829]	27,503 [10321]	1.12	0.32	0.13
Cortical GM (mm^3)	589,195 [88119]	593,792 [87298]	0.99	0.05	0.80
WM (mm^3)	390,902 [87214]	390,349 [101057]	1.00	0.01	0.98
Subcortical GM (mm^3)	35,863 [5650]	36,494 [5129]	0.98	0.12	0.57

Abbreviation; SNHL, Sensorineural hearing loss; NC, Normal control; SD, Standard deviation; CSF, Cerebrospinal fluid; GM, Gray matter; WM, White matter.

(Table 3), and between M–P SNHL and M–P NC participants (Suppl. Table 3). The surface area, thickness, and volumes in cerebral regions according to basic lobar parcellation were not statistically significantly different between SNHL and NC participants (Table 4), and between M–P SNHL and M–P NC participants (Suppl. Table 4).

Fig. 1 shows a cortical thickness map superimposed on a 3-D template brain surface. T-tests demonstrated decreased thickness in the right superior frontal cortex, right lateral orbitofrontal cortex, right superior parietal cortex, left postcentral cortex, left middle occipital cortex (mOC), and left inferior occipital cortex (iOC) on the AAL surface parcellation (Lyttelton et al., 2007) in M–P SNHL compared to age- and gender-matched NC (Fig. 1A). After corrections for multiple comparisons with RFT ($p < 0.02$), the left mOC and left iOC showed significantly reduced cortical thickness in M–P SNHL compared to NC (Fig. 1B). In contrast, when comparing all SNHL (M-M and M–P combined) and NC participants, there was no region that demonstrated statistically significant differences by the *t*-test or by RFT.

Regional surface areas, cortical thicknesses, and cortical volumes of mOC and iOC showed statistically significant differences between M–P SNHL and NC (Table 5, Fig. 2A). Scatter plots of left mOC and left iOC (Fig. 2B) did not show remarkable correlations between regional volumes and age.

4. Discussion

We analyzed region- and surface-based measurements in structural brain MRI of patients with SNHL. The global and lobar cortical surface area, thickness, and volume (Tables 3 and 4, Suppl. Table 3 and 4), global GI (Tables 3, Suppl. 3), and regional volumes (Table 1, Suppl. Table 1), showed no statistically significant differences between SNHL and NC participants. The decreased means of regional cortical thickness and volume in mOC and iOC in M–P SNHL compared to NC participants were statistically significant (Fig. 1, Suppl. Fig. 1).

Table 2
The brain segmental volumes of SNHL and NC participants.

Measurement (ANIMAL segmentation number)	SNHL (N = 30) Mean [SD] (mm^3)	NC (N = 90) Mean [SD] (mm^3)	The rate of SNHL/NC	Absolute Cohen's *d*	*p*
L frontal GM (210)	152,101 [18020]	153,648 [17998]	0.99	0.09	0.68
R frontal GM (211)	153,317 [17972]	153,635 [18350]	1.00	0.02	0.93
L frontal WM (30)	80,851 [18973]	81,330 [22103]	0.99	0.02	0.92
R frontal WM (17)	79,944 [17664]	80,935 [21554]	0.99	0.05	0.82
L temporal GM (218)	100,299 [12321]	101,567 [11816]	0.99	0.11	0.62
R temporal GM (219)	103,185 [12960]	103,425 [12556]	1.00	0.02	0.93
R temporal WM (59)	42,415 [9861]	41,894 [11004]	1.01	0.05	0.82
L temporal WM (83)	42,165 [9991]	41,861 [10295]	1.01	0.03	0.89
L parietal GM (6)	83,756 [11437]	83,779 [10108]	1.00	0	0.99
R parietal GM (2)	82,757 [11477]	82,602 [9487]	1.00	0.02	0.94
L parietal WM (57)	46,283 [9571]	46,236 [11164]	1.00	0	0.98
R parietal WM (105)	45,511 [9339]	45,420 [11226]	1.00	0.01	0.97
L occipital GM (8)	41,611 [7015]	41,856 [5343]	0.99	0.04	0.86
R occipital GM (4)	43,085 [7550]	43,515 [6343]	0.99	0.06	0.76
L occipital WM (73)	21,533 [4934]	21,544 [5279]	1.00	0	0.99
R occipital WM (45)	21,182 [5162]	21,410 [5722]	0.99	0.04	0.85
L thalamus (102)	6966 [796]	7051 [1068]	0.99	0.08	0.69
R thalamus (203)	6939 [794]	7014 [1100]	0.99	0.07	0.73
L caudate (39)	4452 [681]	4677 [1041]	0.95	0.23	0.27
R caudate (53)	4404 [638]	4617 [916]	0.95	0.25	0.24
L fornix (29)	591 [117]	639 [358]	0.93	0.15	0.47
R fornix (254)	573 [112]	605 [271]	0.95	0.13	0.54
L globus pallidus (12)	1052 [150]	1079 [144]	0.97	0.19	0.38
R globus pallidus (11)	1019 [141]	1041 [140]	0.98	0.16	0.46
L putamen (14)	4382 [725]	4401 [654]	1.00	0.03	0.89
R putamen (16)	4426 [712]	4469 [660]	0.99	0.06	0.76
L subthalamic nucleus (33)	45.2 [8.8]	45.7 [9.3]	0.99	0.05	0.80
R subthalamic nucleus (23)	48 [9.48]	47.7 [10.34]	1.01	0.03	0.89
Brainstem (20)	25,427 [4930]	25,839 [4924]	0.98	0.08	0.69
L cerebellum (67)	65,676 [7883]	68,329 [8632]	0.96	0.31	0.14
R cerebellum (76)	65,507 [8206]	68,180 [8903]	0.96	0.31	0.15
L lateral ventricle (3)	4369 [2742]	3579 [2026]	1.22	0.35	0.10
R lateral ventricle (9)	3279 [1736]	3254 [2187]	1.01	0.01	0.96
3rd ventricle (232)	1386 [509]	1163 [389]	1.19	0.53	0.01
4th ventricle (233)	1847 [877]	1718 [733]	1.07	0.17	0.43
Extracerebral CSF (255)	315,599 [93765]	313,333 [99637]	1.01	0.02	0.91

Abbreviation; SNHL, Sensorineural hearing loss; NC, Normal control; SD, Standard deviation; L, left; R, right; GM, gray matter; WM, white matter; CSF, cerebrospinal fluid.

Table 3
The surface based cortical measurements in SNHL and NC participants.

	SNHL (N = 30) Mean [SD]	NC (N = 90) Mean [SD]	The rate of SNHL/NC	Absolute Cohen's *d*	*p*
Gyrification Index	3.79 [0.2]	3.84 [0.17]	0.99	0.28	0.19
L gyrification index	2.75 [0.14]	2.79 [0.13]	0.99	0.32	0.14
R gyrification index	2.79 [0.14]	2.82 [0.12]	0.99	0.18	0.39
L cortex surface area (mm^2)	98,191 [12909]	99,233 [13247]	0.99	0.08	0.71
R cortex surface area (mm^2)	98,571 [12253]	99,289 [13063]	0.99	0.06	0.79
L cortex average thickness (mm)	2.82 [0.32]	2.8 [0.32]	1.01	0.07	0.75
R cortex average thickness (mm)	2.83 [0.34]	2.82 [0.31]	1.01	0.05	0.83
L cortex volume (mm^3)	268,105 [47536]	268,526 [47925]	1.00	0.01	0.97
R cortex volume (mm^3)	268,790 [47067]	270,439 [47338]	0.99	0.03	0.87

Abbreviation; SNHL, Sensorineural hearing loss ; NC, Normal control; SD, standard deviation; L, left hemisphere; R, right hemisphere.

Table 4
The p value in compartments of surface based cortical measurements between SNHL (N = 30) and NC (N = 90) participants.

	Surface area	Cortical thickness	Cortical volume
Frontal lobe, left	0.70	0.70	0.97
Frontal lobe, right	0.61	0.74	0.82
Isthmus lobe, left	0.13	0.88	0.47
Isthmus lobe, right	0.85	0.92	0.85
Parahippocampal lobe, left	0.93	0.74	0.84
Parahippocampal lobe, right	0.93	0.94	0.83
Cingulate lobe, left	0.40	0.64	0.94
Cingulate lobe, right	0.93	0.56	0.72
Temporal lobe, left	0.92	0.70	0.84
Temporal lobe, right	0.88	0.69	0.98
Insula lobe, left	0.58	0.56	0.52
Insula lobe, right	0.92	0.52	0.71
Parietal lobe, left	0.75	0.87	0.96
Parietal lobe, right	0.68	0.93	0.90
Occipital lobe, left	0.48	0.75	0.39
Occipital lobe, right	0.45	0.58	0.30

Abbreviation; SNHL, Sensorineural hearing loss; NC, Normal controls.

4.1. Prior brain morphologic studies in SNHL

Regionally decreased WM volumes were reported in the left posterior superior temporal gyrus (Shibata, 2007), left Heschl's gyrus (Hribar et al., 2014), left middle frontal gyrus (Li et al., 2012), and right iOC (Li et al., 2012). In contrast, morphologic characteristics of gray matter (GM) in SNHL are controversial. Region-based analyses showed no statistically significant changes in global and regional GM surface areas and volumes (Shibata, 2007; Hribar et al., 2014; Li et al., 2012), while a surface-based study in children with SNHL reported decreased cortical thickness in the left precentral gyrus, right postcentral gyrus, left superior occipital gyrus, and the left fusiform gyrus (Li et al., 2012). Additionally, decreased GM volume in the cerebellum was reported in a voxel-based analysis (Hribar et al., 2014).

4.2. Functional distribution of thinner lesions in M–P SNHL

The statistically significantly thinner cortical lesions in M–P SNHL in our study (Fig. 1) correspond to the human motion-sensitive middle temporal area (hMT) (Thiebaut de Schotten et al., 2014), lateral occipital area (LO) (Thiebaut de Schotten et al., 2014; Bona et al., 2015; James et al., 2003), occipital face area (OFA) (Bona et al., 2015; Gauthier et al., 1999), and V8 (Logothetis, 1999; Hadjikhani et al., 1998) in functionally defined cortical areas. Area hMT lies on the posterior bank of the superior temporal sulcus (Thiebaut de Schotten et al., 2014), and processes motion stimuli (Bartels et al., 2008; Fischer et al., 2012). The lateral occipital area extracts general information about an object's structure and plays a role in visual recognition (James et al., 2003; Grill-Spector et al., 2001) and body-part perception (Astafiev et al., 2004). The occipital face area is involved in higher-level face perception, such as identification, emotion and trustworthiness of faces (Bona et al., 2015; Atkinson and Adolphs, 2011). Area V8 is known to be color-sensitive (Logothetis, 1999; Hadjikhani et al., 1998).

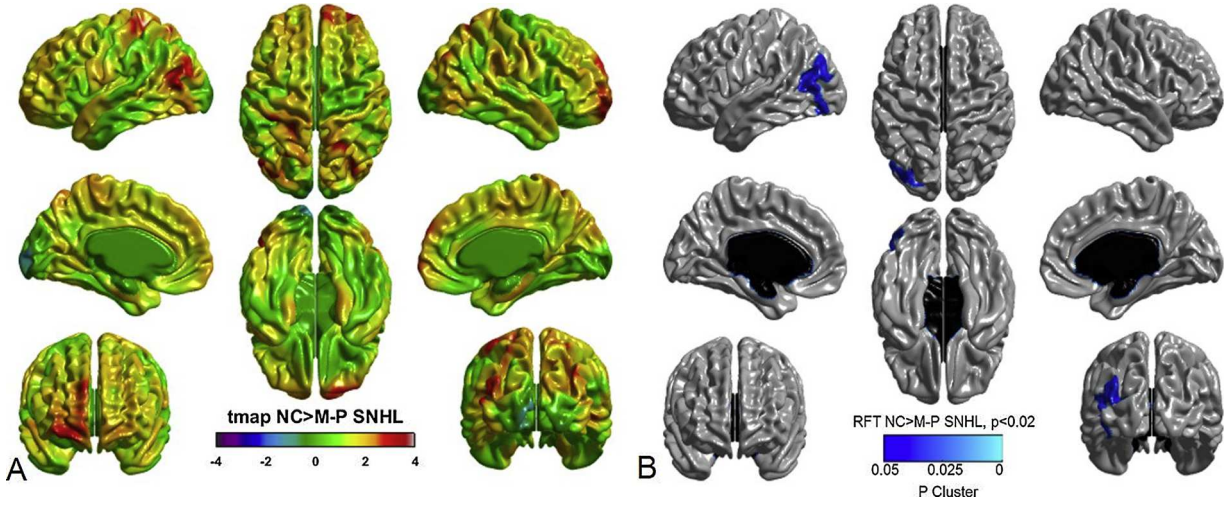

Fig. 1. Visualized cortical thickness with t-statistic map (tmap) (A), and random field theory (RFT) map (B, $p < 0.02$) (corrected for multiple comparisons) showing thicker lesions in moderately severe to profound sensorineural hearing loss (M–P SNHL, N = 12) than normal controls (NC, N = 36). (A) In the color scale, blue and red indicate greater and less mean cortical thicknesses in M–P SNHL, respectively, compared to those in the controls. (B) Blue indicates regions where patients with M–P SNHL had significantly thinner cortex compared to NC at the cluster level corrections for multiple comparisons (For interpretation of the references to colour in this figure legend, the reader is referred to the web version of this article).

Table 5
The cortical measurements of mOC and iOC in M–P SNHL and NC participants.

	M-P SNHL (N = 12) Mean [SD]	NC (N = 36) Mean [SD]	The rate of M-P SNHL/NC	Absolute Cohen's *d*	*p*
mOC, Surface area (mm^2)	4103 [581]	4439 [696]	0.92	0.50	0.139
mOC, Cortical thickness (mm)	2.75 [0.31]	2.93 [0.20]	0.94	0.79	0.021
mOC, Cortical volume (mm^3)	10,362 [2073]	11,968 [2083]	0.87	0.77	0.025
iOC, Surface area (mm^2)	1415 [235]	1617 [272]	0.87	0.77	0.026
iOC, Cortical thickness (mm)	2.69 [0.31]	2.89 [0.27]	0.93	0.70	0.040
iOC, Cortical volume (mm^3)	3764 [771]	4616 [916]	0.82	0.96	0.006

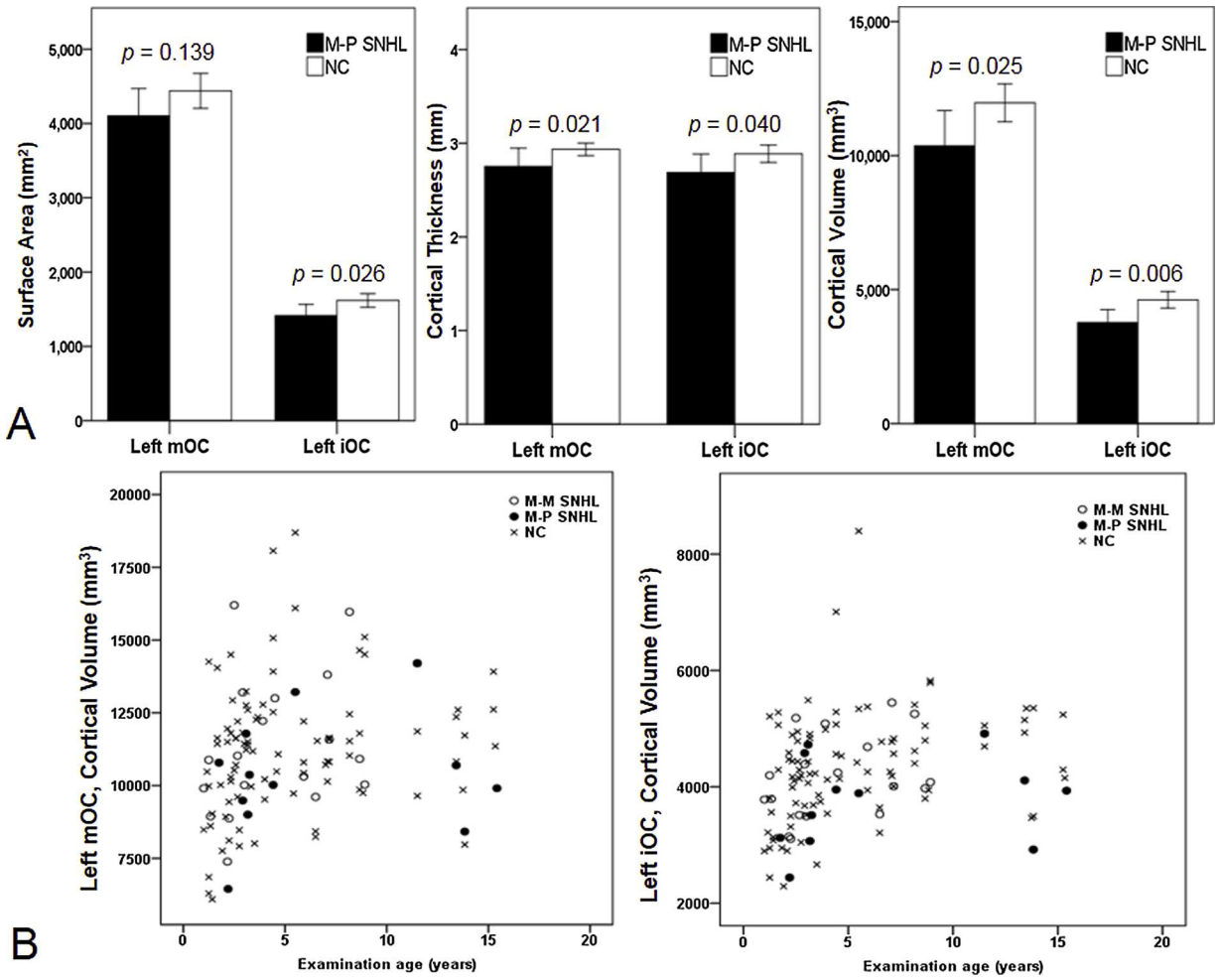

Fig. 2. (A) Column graphs (M–P SNHL vs. NC) showing means of surface areas, cortical thicknesses, and cortical volumes in mOC and iOC. Error bars indicate 95% confidence interval. *p* value were calculated with the *t*-test. (B) Scatter plots (age vs. volume) of left mOC and left iOC. Open circles, closed circles, and cross-marks indicate M-M SNHL, M–P SNHL, and NC, respectively. Abbreviation; M-M, mild to moderate; M–P, moderately severe to profound; SNHL, Sensorineural hearing loss; NC, normal controls; mOC, middle occipital cortex; iOC, inferior occipital cortex.

Taken together, the affected cortical areas in M–P SNHL in our study included areas known to be related to high level visual cognition.

4.3. Audio-visual interaction

Modulations of visual reactivity by auditory inputs have been evidenced in human infants (Watanabe et al., 2013), adults (Vetter et al., 2014; Petro et al., 2017), and mice (Iurilli et al., 2012). Tracer studies in the macaque monkey showed a direct connection between primary visual and auditory areas (Rockland and Ojima, 2003). In humans, functional MRI studies demonstrated cross-sensory activation of the primary visual area (Raij et al., 2010) and LO (Doehrmann et al., 2010; Giovannelli et al., 2016) with the primary auditory area.

In our study, decreased cortical thickness was observed mainly in the lateral occipital part of the visual cortex in M–P SNHL. These M–P SNHL patients received extremely low auditory inputs from prelingual periods prior to medical interventions. The long standing low auditory inputs in the developmental brain may contribute to decreased cortical thickness of extrastriate visual areas in M–P SNHL. Decreased cortical thickness in M–P SNHL may be associated with visual cognitive impairment in SNHL in a clinical setting (Dye and Hauser, 2014; Turgeon et al., 2012).

Regional cortical thickness in the auditory area was not statistically significantly different in SNHL compared to NC in our study (Fig. 1). Similarly, prior brain morphology studies in adult SNHL patients (Shibata, 2007; Hribar et al., 2014) and SNHL children (Li et al., 2012) reported intact GM volumes of the auditory area in agreement with our study. Prior studies have demonstrated that non-auditory sensory

information such as visual and tactile inputs activate the auditory cortex in SNHL (Lomber et al., 2010; Sadato et al., 2005), suggesting substantial plasticity of the auditory cortex during brain development. It may be possible that the auditory cortex in SNHL patients receive atypical inputs from other brain regions such as visuo-spatial information of sign language (Nishimura et al., 1999; Brookshire et al., 2017) to compensate for the loss of auditory signals.

4.4. Limitations

This study has several limitations. First, the possible presence of selection bias (health care access bias) could not be excluded completely, because our study is a retrospective study from a single facility with a relatively small sample size. In terms of SNHL severity, M-M SNHL vs M–P SNHL were 57% vs 43% in a prior cross-section study (Yoshinaga-Itano et al., 2017) and 60% vs 40% in the current study, suggesting that our cohort may be representative of patients with SNHL in other institutions and that our findings might be generalizable to other SNHL patients.

Second, we did not account for congenital cytomegalovirus (CMV) infection. The congenital CMV infection is known as the most common non-genetic cause of childhood SNHL, and is an important pathogen in 10–20% of childhood SNHL (Goderis et al., 2014). In our retrospective study, analysis of medical records indicated that saliva CMV isolation was negative in only 6 of our SNHL patients. We could not completely exclude the possibility that some of the SNHL patients studied here had a congenital CMV infection, which potentially could contribute to the cortical abnormalities observed in this study.

5. Conclusion

We explored brain morphology in 30 SNHL children using region- and surface-based structural MRI analyses. Our data showed no statistically significant difference in global and regional volumes, and global and lobar cortical measurements between SNHL and NC. Comparing M–P SNHL with NC, we found that the regional thickness and volumes in the left mOC, and left iOC on the AAL surface parcellation were reduced in patients with M–P SNHL. In functionally defined cortical areas, the affected lesions corresponded to areas related to high level visual cognition, which suggest that they are potentially associated with visual cognition dysfunction in SNHL.

Author contributions

T.S. was responsible for study design, T.S., J.M., and J.L. analyzed data, and T.S., J.L. and E.T. wrote/edited the manuscript.

Conflict of interest

T.S., J.M., J. L., and E. T. declare relevant no conflicts of interest.

Study funding

This research project was supported by NIHR01HD078561, R21MH118739, R21HD098606, R03NS101372 to E.T., and Natural Science and Engineering Research Council of Canada's Canada Research Chair grant (231266) and Canada Foundation for Innovation and Nova Scotia Research and Innovation Trust infrastructure grant (R0176004) to J.L.

Ethical approval

All procedures performed in studies involving human participants were in accordance with the ethical standards of the institutional and/or national research committee and with the 1964 Helsinki declaration and its later amendments or comparable ethical standards. For this type of study formal consent is not required.

Acknowledge

This research project was supported by NIH R01HD078561, R21MH118739, R21HD098606, R03NS101372 to E.T., and Natural Science and Engineering Research Council of Canada's Canada Research Chair grant (231,266) and Canada Foundation for Innovation and Nova Scotia Research and Innovation Trust infrastructure grant (R0176004) to J.L.

Appendix A. Supplementary data

Supplementary material related to this article can be found, in the online version, at doi:https://doi.org/10.1016/j.ijdevneu.2019.05.009.

References

Centers for Disease Control and Prevention, 2016. Summary of 2016 National CDC Early Hearing Detection and Intervention (EHDI) Data. https://www.cdc.gov/ncbddd/hearingloss/2016-data/01-data-summary.html).

Holzinger, D., Weishaupt, A., Fellinger, P., Beitel, C., Fellinger, J., 2016. Prevalence of 2.2 per mille of significant hearing loss at school age suggests rescreening after NHS. Int. J. Pediatr. Otorhinolaryngol. 87, 121–125.

Swanepoel de, W., Johl, L., Pienaar, D., 2013. Childhood hearing loss and risk profile in a South African population. Int. J. Pediatr. Otorhinolaryngol. 77, 394–398.

Martines, F., Martines, E., Mucia, M., Sciacca, V., Salvago, P., 2013. Prelingual sensorineural hearing loss and infants at risk: western Sicily report. Int. J. Pediatr. Otorhinolaryngol. 77, 513–518.

Monshizadeh, L., Vameghi, R., Sajedi, F., et al., 2018. Comparison of social interaction between cochlear-implanted children with normal intelligence undergoing auditory verbal therapy and normal-hearing children: a pilot study. J. Int. Adv. Otol. 14, 34–38.

Lü, J., Huang, Z., Yang, T., et al., 2011. Screening for delayed-onset hearing loss in preschool children who previously passed the newborn hearing screening. Int. J. Pediatr. Otorhinolaryngol. 75, 1045–1049.

Fitzpatrick, E.M., Dos Santos, J.C., Grandpierre, V., Whittingham, J., 2017. Exploring reasons for late identification of children with early-onset hearing loss. Int. J. Pediatr. Otorhinolaryngol. 100, 160–167.

Tomblin, J.B., Walker, E.A., McCreery, R.W., Arenas, R.M., Harrison, M., Moeller, M.P., 2015. Outcomes of children with hearing loss: data collection and methods. Ear Hear. 36 (Suppl. 1), 14S–23S.

Yoshinaga-Itano, C., Sedey, A.L., Wiggin, M., Chung, W., 2017. Early hearing detection and vocabulary of children with hearing loss. Pediatrics 140, pii:e20162964.

Kronenberger, W.G., Beer, J., Castellanos, I., Pisoni, D.B., Miyamoto, R.T., 2014. Neurocognitive risk in children with cochlear implants. JAMA Otolaryngol. Head Neck Surg. 140, 608–615.

Dye, M.W., Hauser, P.C., 2014. Sustained attention, selective attention and cognitive control in deaf and hearing children. Hear. Res. 309, 94–102.

Turgeon, C., Champoux, F., Lepore, F., Ellemberg, D., 2012. Reduced visual discrimination in cochlear implant users. Neuroreport. 23, 385–389.

Shibata, D.K., 2007. Differences in brain structure in deaf persons on MR imaging studied with voxel-based morphometry. AJNR Am. J. Neuroradiol. 28, 243–249.

Hribar, M., Suput, D., Carvalho, A.A., Battelino, S., Vovk, A., 2014. Structural alterations of brain grey and white matter in early deaf adults. Hear. Res. 318, 1–10.

Li, W., Li, J., Xian, J., et al., 2013. Alterations of grey matter asymmetries in adolescents with prelingual deafness: a combined VBM and cortical thickness analysis. Restor. Neurol. Neurosci. 31, 1–17.

Li, J., Li, W., Xian, J., et al., 2012. Cortical thickness analysis and optimized voxel-based morphometry in children and adolescents with prelingually profound sensorineural hearing loss. Brain Res. 1430, 35–42.

Levman, J., MacDonald, P., Lim, A.R., Forgeron, C., Takahashi, E., 2017. A pediatric structural MRI analysis of healthy brain development from newborns to young adults. Hum. Brain Mapp. 38, 5931–5942.

Pienaar, R., Rannou, N., Bernal, J., Hahn, D., Grant, P.E., 2015. ChRIS–A web-based neuroimaging and informatics system for collecting, organizing, processing, visualizing and sharing of medical data. Conf. Proc. IEEE Eng. Med. Biol. Soc. 2015, 206–209.

Zijdenbos, A.P., Forghani, R., Evans, A.C., 2002. Automatic "pipeline" analysis of 3-D MRI data for clinical trials: application to multiple sclerosis. IEEE Trans. Med. Imaging 21, 1280–1291.

Sherif, T., Kassis, N., Rousseau, M.É, Adalat, R., Evans, A.C., 2015. BrainBrowser: distributed, web-based neurological data visualization. Front. Neuroinform. 8, 89.

Sled, J.G., Zijdenbos, A.P., Evans, A.C., 1998. A nonparametric method for automatic correction of intensity nonuniformity in MRI data. IEEE Trans. Med. Imaging 17, 87–97.

Fonov, V.S., Evans, A.C., McKinstry, R.C., Almli, C.R., Collins, D.L.L., 2009. Unbiased nonlinear average age-appropriate brain templates from birth to adulthood. NeuroImage. 47, S102. http://www.sciencedirect.com/science/article/pii/S1053811909708845).

Smith, S.M., 2002. Fast robust automated brain extraction. Hum. Brain Mapp. 17, 143–155.
Tohka, J., Zijdenbos, A., Evans, A., 2004. Fast and robust parameter estimation for statistical partial volume models in brain MRI. Neuroimage. 23, 84–97.
Collins, D.L., Zijdenbos, A.P., Baaré, W.F.C., Evans, A.C., 1999. ANIMAL+INSECT: improved cortical structure segmentation. In: Kuba, A., Šáamal, M., Todd-Pokropek, A. (Eds.), Information Processing in Medical Imaging. Lecture Notes in Computer Science. Springer, Berlin, Heidelberg, pp. 210–223 1613.
Kim, J.S., Singh, V., Lee, J.K., et al., 2005. Automated 3-D extraction and evaluation of the inner and outer cortical surfaces using a Laplacian map and partial volume effect classification. Neuroimage. 27, 210–221.
Boucher, M., Whitesides, S., Evans, A., 2009. Depth potential function for folding pattern representation, registration, and analysis. Med. Image Anal. 13, 203–214.
Lyttelton, O., Boucher, M., Robbins, S., Evans, A., 2007. An unbiased iterative group registration template for cortical surface analysis. Neuroimage. 34, 1535–1544.
Benjamini, Y., Drai, D., Elmer, G., Kafkafi, N., Golani, I., 2001. Controlling the false discovery rate in behavior genetics research. Behav. Brain Res. 125, 279–284.
Thiebaut de Schotten, M., Urbanski, M., Valabregue, R., Bayle, D.J., Volle, E., 2014. Subdivision of the occipital lobes: an anatomical and functional MRI connectivity study. Cortex. 56, 121–137.
Bona, S., Cattaneo, Z., Silvanto, J., 2015. The causal role of the occipital face area (OFA) and lateral occipital (LO) cortex in symmetry perception. J. Neurosci. 35, 731–738.
James, T.W., Culham, J., Humphrey, G.K., Milner, A.D., Goodale, M.A., 2003. Ventral occipital lesions impair object recognition but not object-directed grasping: an fMRI study. Brain 126, 2463–2475.
Gauthier, I., Tarr, M.J., Anderson, A.W., Skudlarski, P., Gore, J.C., 1999. Activation of the middle fusiform' face area' increases with expertise in recognizing novel objects. Nat. Neurosci. 2, 568–573.
Logothetis, N.K., 1999. Vision: a window on consciousness. Sci. Am. 281, 69.
Hadjikhani, N., Liu, A.K., Dale, A.M., Cavanagh, P., Tootell, R.B., 1998. Retinotopy and color sensitivity in human visual cortical area V8. Nat. Neurosci. 1, 235–241.
Bartels, A., Logothetis, N.K., Moutoussis, K., 2008. fMRI and its interpretations: an illustration on directional selectivity in area V5/MT. Trends Neurosci. 31, 444–453.
Fischer, E., Bülthoff, H.H., Logothetis, N.K., Bartels, A., 2012. Visual motion responses in the posterior cingulate sulcus: a comparison to V5/MT and MST. Cereb. Cortex 22, 865–876.
Grill-Spector, K., Kourtzi, Z., Kanwisher, N., 2001. The lateral occipital complex and its role in object recognition. Vision Res. 41, 1409–1422.
Astafiev, S.V., Stanley, C.M., Shulman, G.L., Corbetta, M., 2004. Extrastriate body area in human occipital cortex responds to the performance of motor actions. Nat. Neurosci. 7, 542–548.
Atkinson, A.P., Adolphs, R., 2011. The neuropsychology of face perception: beyond simple dissociations and functional selectivity. Philos. Trans. R. Soc. Lond., B, Biol. Sci. 366, 1726–1738.
Watanabe, H., Homae, F., Nakano, T., et al., 2013. Effect of auditory input on activations in infant diverse cortical regions during audiovisual processing. Hum. Brain Mapp. 34, 543–565.
Vetter, P., Smith, F.W., Muckli, L., 2014. Decoding sound and imagery content in early visual cortex. Curr. Biol. 24, 1256–1262.
Petro, L.S., Paton, A.T., Muckli, L., 2017. Contextual modulation of primary visual cortex by auditory signals. Philos. Trans. R. Soc. Lond., B, Biol. Sci. 372, 1714.
Iurilli, G., Ghezzi, D., Olcese, U., et al., 2012. Sound-driven synaptic inhibition in primary visual cortex. Neuron. 73, 814–828.
Rockland, K.S., Ojima, H., 2003. Multisensory convergence in calcarine visual areas in macaque monkey. Int. J. Psychophysiol. 50, 19–26.
Raij, T., Ahveninen, J., Lin, F.H., et al., 2010. Onset timing of cross-sensory activations and multisensory interactions in auditory and visual sensory cortices. Eur. J. Neurosci. 31, 1772–1782.
Doehrmann, O., Weigelt, S., Altmann, C.F., Kaiser, J., Naumer, M.J., 2010. Audiovisual functional magnetic resonance imaging adaptation reveals multisensory integration effects in object-related sensory cortices. J. Neurosci. 30, 3370–3379.
Giovannelli, F., Giganti, F., Righi, S., et al., 2016. Audio-visual integration effect in lateral occipital cortex during an object recognition task: an interference pilot study. Brain Stimul. 9, 574–576.
Lomber, S.G., Meredith, M.A., Kral, A., 2010. Cross-modal plasticity in specific auditory cortices underlies visual compensations in the deaf. Nat. Neurosci. 13, 1421–1427.
Sadato, N., Okada, T., Honda, M., et al., 2005. Cross-modal integration and plastic changes revealed by lip movement, random-dot motion and sign languages in the hearing and deaf. Cereb. Cortex 15, 1113–1122.
Nishimura, H., Hashikawa, K., Doi, K., et al., 1999. Sign language' heard' in the auditory cortex. Nature. 397, 116.
Brookshire, G., Lu, J., Nusbaum, H.C., Goldin-Meadow, S., Casasanto, D., 2017. Visual cortex entrains to sign language. Proc. Natl. Acad. Sci. U. S. A. 114, 6352–6357.
Goderis, J., De Leenheer, E., Smets, K., Van Hoecke, H., Keymeulen, A., Dhooge, I., 2014. Hearing loss and congenital CMV infection: a systematic review. Pediatrics. 134, 972–982.